

A Feature-based Inversion Method for Brain Stroke Microwave Imaging

Rui Guo⁽¹⁾, Zhichao Lin⁽¹⁾, Jingyu Xin⁽¹⁾, Maokun Li⁽¹⁾,
Fan Yang⁽¹⁾, Shenheng Xu⁽¹⁾, and Aria Abubakar⁽²⁾

(1) Tsinghua University, Beijing, China; e-mail: guor93@tsinghua.edu.cn; maokunli@tsinghua.edu.cn

(2) SLB, Houston, TX, USA; e-mail: aabubakar@slb.com

Abstract

We propose an inversion method in the feature space to reconstruct human heads' three-dimensional (3-D) permittivity and conductivity distribution for brain stroke microwave imaging. The permittivity and conductivity distribution of human heads are compressed into latent codes of a variational autoencoder (VAE). The optimal codes are solved during the inversion process by minimizing a regularized cost function using iterative optimization. The final head model will be decoded from the decoder of the VAE. This method seamlessly incorporates the prior knowledge of brain structures into the imaging process and significantly reduces the number of unknowns. Numerical experiments show that it can achieve higher resolution with a faster solution speed than the conventional voxel-based method.

1 Introduction

Microwave imaging is an effective tool for early diagnosis and bedside monitoring of brain strokes[1]. It is portable, non-invasive, and harmless to human bodies. The basic principle is that the permittivity and conductivity of brain tissues are different. Electromagnetic fields measured outside the head can be inverted to the spatial distribution of the electrical properties, according to which hemorrhagic or ischemic injuries can be located.

Quantitatively recovering the permittivity and conductivity relies on solving a nonlinear inverse scattering problem. The optimal electrical parameters are found by minimizing the misfit between the simulated data and the measurements. This inverse problem is challenging due to high nonlinearity, ill-posedness, and computational complexity. Most algorithms divide the imaging domain into pixels or voxels[1][2], and the number of unknowns is usually larger than the data volume. Prior knowledge described by regularizations is required to stabilize the solution process. However, most regularization schemes are handcrafted and only constrain the unknowns at the pixel or voxel level. The common structural information of human brains is absent in the inversion process; therefore, the imaging resolution is generally limited.

Data-driven deep learning approaches can overcome the limitations of handcrafted regularizations and accelerate the online imaging process[3][4]. However, there are still

bottlenecks in 3-D brain imaging. First, the cost of offline training is immense. Full-wave simulations of 3-D heads to construct the training set are time- and memory-consuming, and training a deep neural network whose output may have millions of unknowns is resource-consuming. Second, data-driven methods suffer from risks of misdiagnosis. A surrogate model deduced from specific datasets may not be able to predict diverse human brains.

In this work, the 3-D head's permittivity and conductivity are compressed into latent codes in the feature space of a VAE. The optimal codes are solved in the physics-based deterministic framework, where the data misfit between the simulated data and the measurements is minimized. Numerical examples show that this method improves imaging resolution and computational speed compared with the conventional voxel-based method.

2 Strategy of encoding and decoding

A VAE is constructed to transform the 3-D brain between voxels and codes. It contains an encoder and a decoder[5]. The encoder converts the brain to a distribution of latent codes corresponding to the posterior probability of training data. The decoder recovers the sampled code vector from the distribution to a brain. The VAE has a continuous and complete latent space for stably optimizing the codes in data inversion.

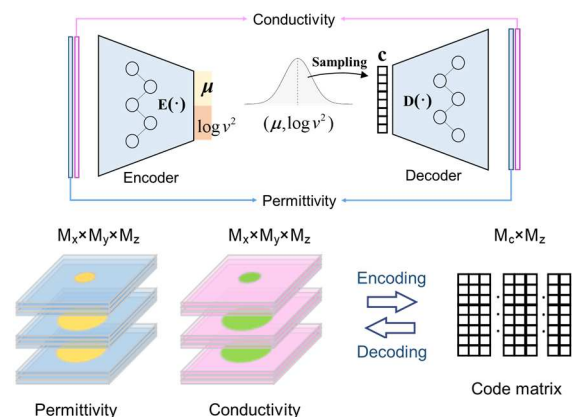


Figure 1. An illustration of 3-D head compression by the 2-D VAE. The VAE is trained to compress two-channel real-valued images into code vectors. 3-D heads can be represented by a code matrix with each column representing a transverse slice.

As shown in Figure 1, the 2-D VAE is applied to compress 3-D heads. Its input is a $M_x \times M_y \times 2$ image that represents the transverse plane of a head, which is composed of two channels related to the permittivity and conductivity. The encoder converts the input to the mean and logarithmic variance of the code vector, whose size is $M_c \times 1$. The decoder will sample from the distribution and recover the input from the sample codes. To compress a 3-D model consisting of $M_x \times M_y \times M_z$ voxels, the above procedure will be performed M_z times for all transverse planes. The final codes will be an $M_c \times M_z$ matrix with each column representing a transverse slice. Finally, the complex permittivity of a 3-D head can be represented by latent codes in the VAE's feature space:

$$\mathbf{m} = D(\mathbf{c}), \quad (1)$$

where \mathbf{m} is the discrete complex permittivity represented by voxels, \mathbf{c} is the code vector for all transverse slices, and D is the decoder.

3 Inversion algorithm

Let us denote the forward problem as

$$\mathbf{d} = F(\mathbf{m}) = G(\mathbf{c}), \quad (2)$$

where F is the electromagnetic simulation function, \mathbf{d} is the simulated microwave data, and G builds the connection between the data and codes.

The cost function for inversion is defined as

$$L(\mathbf{c}) = \alpha_d \|\mathbf{d}_{\text{obs}} - G(\mathbf{c})\|^2 + \alpha_z \|\nabla_z G(\mathbf{c})\|^2, \quad (3)$$

where \mathbf{d}_{obs} is the observed data, ∇_z is the differential operator along the z -direction, α_d and α_z are factors that balance the weight of the two terms. The regularization ensures that the decoded permittivity and conductivity are continuous in the vertical direction.

Equation (3) is minimized by the Gauss-Newton method. In the k th iteration, the update of codes, $\Delta \mathbf{c}_k$, is solved from

$$\mathbf{A} \Delta \mathbf{c}_k = \mathbf{b} \quad (4)$$

with

$$\mathbf{A} = \alpha_d \mathbf{J}_d^H \mathbf{J}_d + \alpha_z \mathbf{J}_d^H \nabla_z^T \nabla_z \mathbf{J}_d + \beta \mathbf{I}, \quad (5)$$

$$\mathbf{b} = \alpha_d \mathbf{J}_d^H (\mathbf{d}_{\text{obs}} - G(\mathbf{c}_{k-1})) - \alpha_z \mathbf{J}_d^H \nabla_z^T \nabla_z D(\mathbf{c}_{k-1}), \quad (6)$$

where \mathbf{J}_d and \mathbf{J}_g are the Jacobian matrix of the decoder D and the forward problem G , \mathbf{I} is the identity matrix, and β is the Tikhonov regularization factor.

The elements of \mathbf{J}_d are partial derivatives of \mathbf{m} to the latent vector \mathbf{c} . They are computed by the finite-difference method, i.e.,

$$\frac{\partial \mathbf{m}}{\partial c_i} \approx \frac{D(\mathbf{c} + \delta_i) - D(\mathbf{c})}{\delta_i} \quad (7)$$

where c_i is the i -th element of the vector, and δ_i is a small value that perturbs c_i .

The elements of \mathbf{J}_g are sensitivities of measurements to the latent codes, which are computed according to the chain rule:

$$\frac{\partial \mathbf{d}(\mathbf{r}_0)}{\partial c_i} = \sum_{l=1}^{M_x \times M_y} \frac{\partial m_l}{\partial c_i} \frac{\partial \mathbf{d}(\mathbf{r}_0)}{\partial m_l} \quad (8)$$

where the last term is the sensitivity of the microwave data at the location \mathbf{r}_0 with respect to the l -th element of \mathbf{m} , which can be computed by the adjoint equation method.

Computing the forward modeling and Fréchet derivatives are accelerated on multiple GPUs. First, all perturbed codes of a transverse slice are aligned as a 2-D matrix, which will be taken as a batch to input the decoder. The prediction is naturally parallelized under the deep learning framework. Second, microwave fields generated by different sources are computed and stored in parallel, which enables us to independently compute equation (8) for different transmitting-receiving pairs on multiple GPUs.

4 Numerical experiments

4.1 Dataset Preparation

The 3-D head models are constructed based on an open-source MRI dataset [6]. Most MRI models have a resolution of 1 mm^3 . The dataset also contains lesion volumes labeled for each patient.

The heads are segmented into five classes: white matter, gray matter, cerebrospinal fluid (CSF), skull, and other parts. Strokes are simulated by labeled lesions and circles generated by ourselves. Different values of complex permittivity are assigned to the five classes according to the Gaussian distribution shown in Table 1.

Table 1. Complex permittivity of the numerical head.

Class	Real part*	Imaginary part @ 1GHz*
Skull	(8, 0.3)	(3, 0.3)
White matter	(40, 1.0)	(11, 1.0)
Gray matter	(52, 1.0)	(17, 1.0)
CSF	(63, 1.5)	(44, 1.5)
Hemorrhagic - stroke	(60, 1.0)	(17, 1.0)
Ischemic - stroke	(35, 1.0)	(15, 1.0)
Other	(44, 0.3)	(17, 0.3)

*The first and second terms in parentheses correspond to the mean and standard deviation of the Gaussian distribution.

Thirty human heads are processed in total. Twenty-five heads are used for training the VAE. The other five heads are used for validating the VAE and the data inversion algorithm.

4.2 Training and Test of the VAE

The VAE is trained self-supervised. The loss function is[5]

$$l = \frac{1}{M_x \times M_y} \sum_{i=1}^2 \sum_{l=1}^{M_x \times M_y} (m_i - \tilde{m}_i)^2 - \lambda \sum_{q=1}^Q (1 + \log v_q^2 - \mu_q^2 - v_q^2), \quad (9)$$

where m is the label, \tilde{m} is the output of the VAE, μ and v is the mean and variance of the encoded Gaussian distribution, respectively, Q is the length of the code vector, and λ is the regularization factor.

Among the 125,000 images generated based on the twenty-five heads, 90% and 10% are used for training and testing, respectively. We set the length of the code vector to 96, the number of training epochs to 20, and the size of input batch to 60. The starting learning rate is $5e^{-5}$ and decays exponentially. The average reconstruction loss of a training, test, and validation batch are 12.3, 14.3, and 14.5, respectively. It indicates that the VAE can encode and decode accurately without overfitting.

4.3 Brain Stroke Imaging

The test 3-D head models are discretized by $300 \times 300 \times 300$ voxels for electromagnetic modeling. There are seven circles of antennas around the head, the number of antennas being 8, 8, 8, 12, 14, 14, and 14 from top to bottom. FDTD method is applied to simulate the measurement. 5% Gaussian white noise is added to the simulated data. The inversion frequency is 0.8, 0.9, and 1.0 GHz.

The first example shows the reconstruction of a normal head. The true distribution of complex permittivity on the transverse, sagittal, and coronal plane is shown in Figure 2.

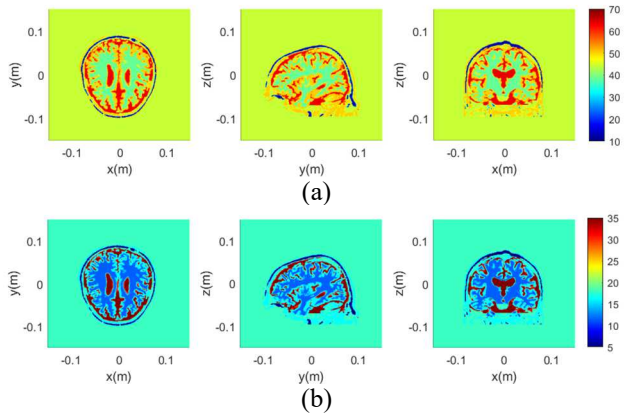


Figure 2. The ground truth of a normal head. (a) Real part of complex permittivity. (b) Imaginary part of complex permittivity.

Inversion results using the proposed method and the voxel-based method are shown in Figure 3 and Figure 4, respectively. Both methods adopt a $100 \times 100 \times 100$ mesh for forward modeling and inversion. It is observed that the structural information in Figure 3 is much clearer than that in Figure 4. The structural similarity (SSIM) with the

ground truth of the two methods is 0.76 and 0.67, respectively.

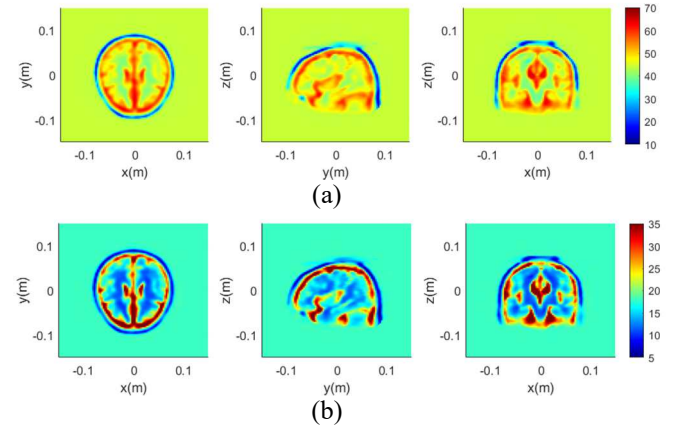


Figure 3. Reconstructed permittivity of the proposed method (normal head). (a) Real part of complex permittivity. (b) Imaginary part of complex permittivity.

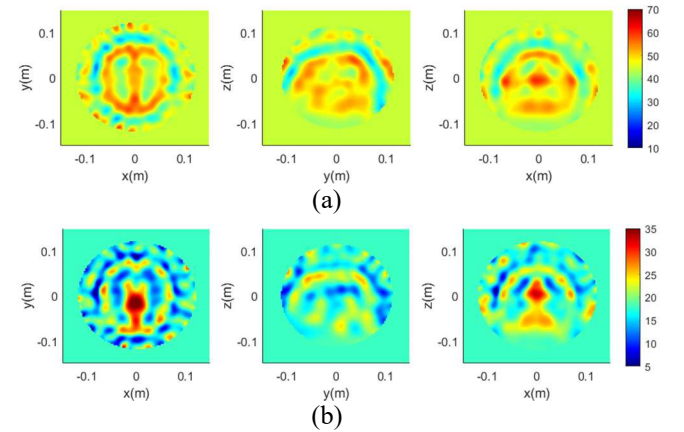


Figure 4. Reconstructed permittivity of the voxel-based method (normal head). (a) Real part of complex permittivity. (b) Imaginary part of complex permittivity.

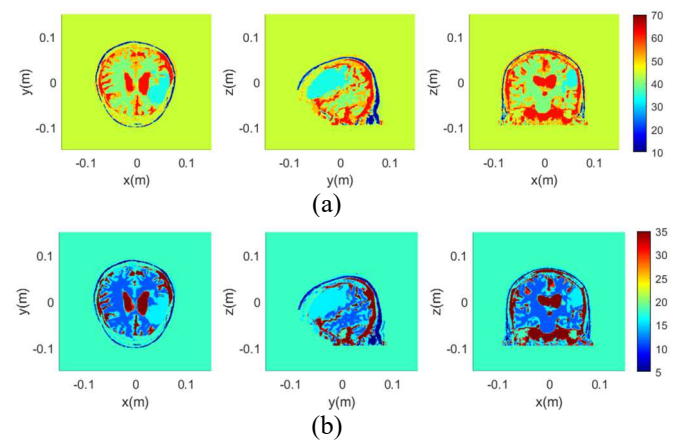


Figure 5. The ground truth of an ischemic stroke head. (a) Real part of complex permittivity. (b) Imaginary part of complex permittivity.

The second example shows the reconstruction of an ischemic stroke head. The transverse, sagittal, and coronal planes of the head are shown in Figure 5. The complex permittivity of the stroke is 33.9-15.8j.

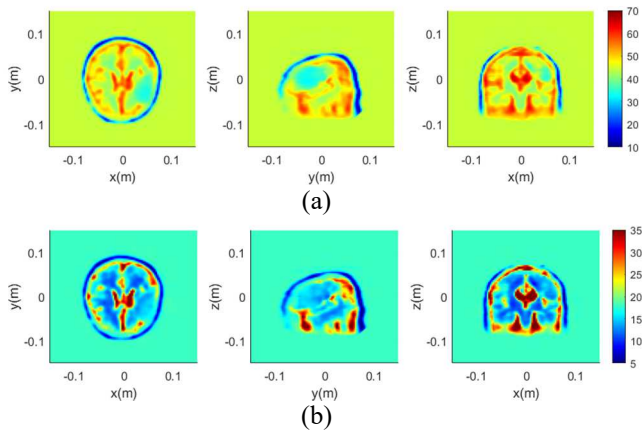


Figure 6. Reconstructed permittivity of the proposed method (ischemic stroke). (a) Real part of complex permittivity. (b) Imaginary part of complex permittivity.

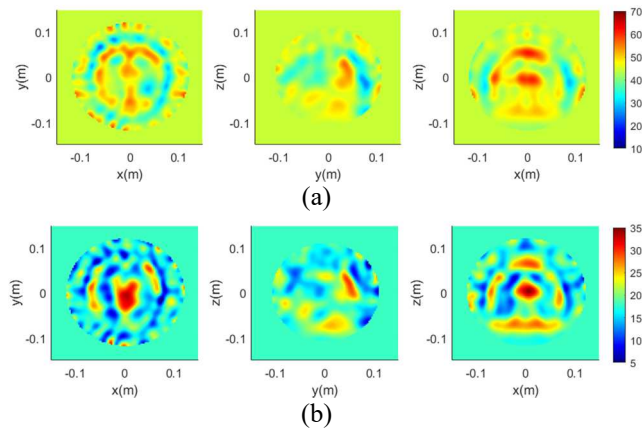


Figure 7. Reconstructed permittivity of the voxel-based method (ischemic stroke). (a) Real part of complex permittivity. (b) Imaginary part of complex permittivity.

Inversion results of the ischemic stroke using the proposed method and voxel-based method are shown in Figure 6 and Figure 7, respectively. Both methods show the existence of the stroke, but the proposed method can recover the structure and electrical properties more accurately. It is also observed that the conductivity image of the voxel-based method is difficult to be used for stroke evaluation. The SSIM of the two methods is 0.75 and 0.62.

The proposed method significantly reduces the number of unknowns and accelerates the imaging process. For instance, the number of unknowns in the two methods is 19600 and 268069, respectively. The time of solving the matrix equation is 0.08s and 200s, respectively. Inversion in the feature space achieves a 3.6% compression rate and four-order acceleration.

5 Conclusion

We propose a microwave data inversion method in feature space for brain stroke imaging. The VAE is applied to compress voxel-based heads into latent codes in the feature space. A dataset of head models characterized by permittivity and conductivity is constructed from MRI images for training and validation. In data inversion, the optimal codes are sought by minimizing a regularized data misfit function. Parallelization on GPUs is applied to accelerate the inversion algorithm. Compared with the conventional voxel-based method, the proposed method can achieve a nearly 25% higher structural similarity and four-order acceleration of the solution process using a 3.6% number of unknowns.

Acknowledgements

This work was supported in part by the China Postdoctoral Science Foundation (2022M721778), Shuimu Tsinghua Scholar Program of Tsinghua University (2021SM031), National Natural Science Foundation of China (42204109, 61971263, and 62171259).

References

- [1] M. Hopfer, R. Planas, A. Hamidipour, T. Henriksson, and S. Semenov, "Electromagnetic tomography for detection, differentiation, and monitoring of brain stroke: A virtual data and human head phantom study," *IEEE Antennas and Propagation Magazine*, vol. 59, no. 5, pp. 86–97, 2017.
- [2] I. Bisio, C. Estatico, A. Fedeli, F. Lavagetto, M. Pastorino, A. Randazzo, and A. Sciarrone, "Variable-exponent lebesgue-space inversion for brain stroke microwave imaging," *IEEE Transactions on Microwave Theory and Techniques*, vol. 68, no. 5, pp. 1882–1895, 2020.
- [3] X. Ye, N. Du, D. Yang, X. Yuan, R. Song, S. Sun, and D. Fang, "Application of generative adversarial network-based inversion algorithm in imaging 2-D lossy biaxial anisotropic scatterer," *IEEE Transactions on Antennas and Propagation*, vol. 70, no. 9, pp. 8262–8275, 2022.
- [4] M. Li, R. Guo, K. Zhang, Z. Lin, F. Yang, S. Xu, X. Chen, A. Massa, and A. Abubakar, "Machine learning in electromagnetics with applications to biomedical imaging: A review," *IEEE Antennas and Propagation Magazine*, vol. 63, no. 3, pp. 39–51, 2021.
- [5] D. P. Kingma and M. Welling, "Auto-encoding variational Bayes," *arXiv preprint arXiv:1312.6114*, 2013.
- [6] S.-L. Liew, J. M. Anglin, N. W. Banks, M. Sondag, K. L. Ito, H. Kim, J. Chan, J. Ito, C. Jung, N. Khoshab, et al., "A large, open source dataset of stroke anatomical brain images and manual lesion segmentations," *Scientific data*, vol. 5, no. 1, pp. 1–11, 2018.